Catalysis Letters (2020) 150:1527–1536
https://doi.org/10.1007/s10562-019-03051-8

Ni–Zn–Al-Based Oxide/Spinel Nanostructures for High Performance, Methane-Selective CO_2 Hydrogenation Reactions

T. Rajkumar[1] · András Sápi[1,2] · Marietta Ábel[1] · Ferenc Farkas[3] · Juan Fernando Gómez-Pérez[1] · Ákos Kukovecz[1] · Zoltán Kónya[1,4]

Received: 3 November 2019 / Accepted: 21 November 2019 / Published online: 7 December 2019

Abstract

In the present study, NiO modified $ZnAl_2O_4$ and ZnO modified $NiAl_2O_4$ spinel along with pure Al_2O_3, $ZnAl_2O_4$ and $NiAl_2O_4$ for comparison in the CO_2 hydrogenation reaction have been investigated. It was found that $NiAl_2O_4$, $NiO/ZnAl_2O_4$ and $ZnO/NiAl_2O_4$ catalysts exhibited outstanding activity and selectivity towards methane even at high temperature compared to similar spinel structures reported in the literature. $NiO/ZnAl_2O_4$ catalyst showed CO_2 consumption rate of ~ 19 µmol/g·s at 600 °C and ~ 85% as well as ~ 50% of methane selectivity at 450 °C and 600 °C, respectively. The high activity and selectivity of methane can be attributed to the presence of metallic Ni and $Ni/NiO/ZnAl_2O_4$ interface under the reaction conditions as evidenced by the XRD results.

Graphic Abstract

High performance Ni–Zn–Al-based oxide/spinel nanostructures is synthesized and $NiO/ZnAl_2O_4$ catalyst exhibited higher catalytic activity in the CO_2 hydrogenation reaction due to the presence of metal support interaction between Ni and $ZnAl_2O_4$ support.

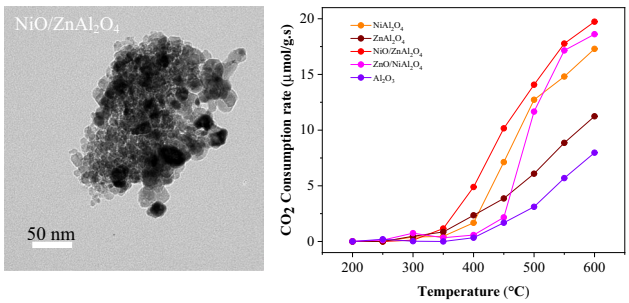

Keywords Spinel · Co-precipitation method · XRD · TGA · TEM · CO_2 hydrogenation

✉ András Sápi
sapia@chem.u-szeged.hu

1 Department of Applied and Environmental Chemistry, Interdisciplinary Excellence Centre, University of Szeged, Rerrich Béla tér 1, Szeged 6720, Hungary

2 Institute of Environmental and Technological Sciences, University of Szeged, Szeged 6720, Hungary

3 Department of Technology, Faculty of Engineering, University of Szeged, Mars tér 7, Szeged 6724, Hungary

4 MTA-SZTE Reaction Kinetics and Surface Chemistry Research Group, University of Szeged, Szeged 6720, Hungary

1 Introduction

The catalytic conversion of CO_2 is desirable strategy to not only reduce the CO_2 emission but also to produce useful chemicals/fuels [1, 2]. Depending upon the catalysts used, different kinds of products were obtained such as CO via reverse water gas shift (RWGS) reaction, methane (Sabatier reaction) and methanol [3–5]. The obtained CO in the RWGS reaction can be converted into value added chemicals through Fischer–Tropsch synthesis. RWGS is endothermic ($CO_2 + H_2 \leftrightarrow CO + H_2O$, $\Delta H_{RWGS} = +41$ kJ/mol)

and thermodynamically favoured at high temperatures [6]. Cu [7], Pt [8] and Rh [9] on various supports have been reported as the most active catalysts for RWGS reaction. Methanation is exothermic ($CO_2 + 4H_2 \rightarrow CH_4 + 2H_2O$, $\Delta H_{Sab} = -165$ kJ/mol) and thermodynamically favoured at low temperatures [10]. Ni [11], Ru [4] and Rh [12] are most widely used catalysts for CO_2 methanation reaction. Cu [13] and Pd [14] are most widely used catalysts for the reduction of CO_2 to methanol [15–17]. Nickel based catalysts have been widely investigated as catalyst in CO_2 hydrogenation reactions owing to its superior catalytic activity and low cost [18, 19]. Recently, nickel based spinel catalysts have been widely used in CO_2 hydrogenation reaction due to their low cost and superior catalytic activity [20–22]. Further, they were also used in other fields such as in adsorption [23], sensors [24] and as flexible materials [25]. They have also been used as catalyst support due to its low reactivity with the active phase and its high resistance to high temperatures and acidic or basic atmospheres [26]. Interestingly, $NiAl_2O_4$ was found to minimize the coke formation in CO_2 reforming of methane [27]. Besides nickel based spinels, zinc based spinels were also used in various fields such as in catalysis [15, 28–30], adsorption [31] and optics [32] due to their superior catalytic activity and high thermal stability [33]. However, the catalytic applications of these spinel materials for CO_2 hydrogenation is not reported. In the present study, various Nickel–Zinc–Aluminum-based spinels as well as oxide/spinel catalysts were produced where the position of the nickel and zinc atoms or ions were changed. The catalysts were characterized by XRD, N_2 physisorption, TEM, SEM–EDX and TGA. These catalysts were tested in CO_2 hydrogenation reaction in the gas phase. It was found that $NiAl_2O_4$, $NiO/ZnAl_2O_4$ and $ZnO/NiAl_2O_4$ catalysts during the reaction conditions exhibited outstanding activity and selectivity towards methane even at high temperature as these catalysts comprise metallic nanoparticles in their structure. Among these catalysts, $NiO/ZnAl_2O_4$ catalyst showed CO_2 consumption rate of ~ 19 µmol/g s at 600 °C and ~ 85% as well as ~ 50% of methane selectivity at 450 °C and 600 °C, respectively.

2 Experimental details

2.1 Chemicals

$Zn(NO_3)_2{\cdot}6H_2O$ (≥ 99%) and $Al(NO_3)_3{\cdot}9H_2O$ (≥ 98%) were purchased from Sigma-Aldrich. Aqueous ammonia solution was purchased from Molar chemicals. $Ni(NO_3)_2{\cdot}6H_2O$ was purchased from Merck.

2.2 Catalyst Preparation

The $ZnAl_2O_4$ oxide was synthesized by a co-precipitation method in accordance with the procedure reported in the previous work [34]. Typically, appropriate amount of $Zn(NO_3)_2{\cdot}6H_2O$ and $Al(NO_3)_3{\cdot}9H_2O$ with a molar ratio of 1:2 were dissolved in 100 mL deionized water. Then, an aqueous ammonia solution was added dropwise into the mixed solution at room temperature until pH value of about 7. The obtained precipitate was aged for 2 h at 70 °C. Then, the solid product was recovered by filtration, washing with deionized water and drying overnight at 100 °C. The $ZnAl_2O_4$ was obtained after calcination in air at 500 °C for 5 h. The $NiAl_2O_4$ and pure Al_2O_3 were prepared by the same procedure using their corresponding metal nitrate precursors. In order to investigate the interphase effect of metal cations present in the $ZnAl_2O_4$ and $NiAl_2O_4$ spinels, we loaded exactly the amount of ZnO present in $ZnAl_2O_4$ onto $NiAl_2O_4$ and vice versa. Based on the calculation, we loaded 44wt% of ZnO on $NiAl_2O_4$ and represented as $ZnO/NiAl_2O_4$ and 42wt% of NiO on $ZnAl_2O_4$ and represented as $NiO/ZnAl_2O_4$.

2.3 Catalyst Characterization

2.3.1 N_2 Adsorption–Desorption Isotherm Measurements

The specific surface area (BET method), the pore size distribution and the total pore volume were determined by the BJH method using a Quantachrome NOVA 2200 gas sorption analyzer by N_2 gas adsorption/desorption at − 196 °C. Before the measurements, the samples were pre-treated in a vacuum (< ~ 0.1 mbar) at 200 °C for 2 h.

2.3.2 Powder X-ray Diffraction (XRD)

XRD studies of all samples were performed on a Rigaku MiniFlex II instrument with a Ni-filtered CuKα source in the range of 2θ = 10–80°.

2.3.3 Thermogravimetric Analysis (TGA)

Thermogravimetric analysis was obtained using TAQ500 instruments under flow of air from room temperature to 800 °C at a heating rate of 10 °C min^{-1}.

2.3.4 Scanning Electron Microscopy (SEM–EDX)

Scanning electron microscopy equipped with an energy dispersive X-ray spectroscopy (Hitachi S-4700) was applied at 20 kV on the samples.

2.3.5 Transmission Electron Microscopy (TEM)

Imaging of the all the samples were carried out using an FEI TECNAI G2 20 X-Twin high-resolution transmission electron microscope (equipped with electron diffraction) operating at an accelerating voltage of 200 kV. The samples were drop-cast onto carbon film coated copper grids from ethanol suspension.

2.4 Catalytic Activity Studies

2.4.1 Hydrogenation of Carbon-dioxide in a Continuous Flow Reactor

Before the catalytic experiments, the as-received catalysts were oxidized in O_2 atmosphere at 300 °C for 30 min and thereafter were reduced in H_2 at 300 °C for 60 min. Catalytic reactions were carried out at atmospheric pressure in a fixed-bed continuous-flow reactor (200 mm long with 8 mm i.d.) which was heated externally. The dead volume of the reactor was filled with quartz beads. The operating temperature was controlled by a thermocouple placed inside the oven close to the reactor wall, to assure precise temperature measurement. For catalytic studies, small fragments (about 1 mm) of slightly compressed pellets were used. Typically, the reactor filling contained 150 mg of catalyst. In the reacting gas mixture, the CO_2:H_2 molar ratio was 1:4, if not denoted otherwise. The CO_2:H_2 mixture was fed with the help of mass flow controllers (Aalborg), the total flow rate was 50 ml/min. The reacting gas mixture flow entered and left the reactor through an externally heated tube in order to avoid condensation. The analysis of the products and reactants was performed with an Agilent 6890 N gas chromatograph using HP-PLOTQ column. The gases were detected simultaneously by thermal conductivity (TC) and flame ionization (FI) detectors. The CO_2 was transformed by a methanizer to methane and it was also analysed by FID. CO_2 conversion was calculated on a carbon atom basis, i.e.

$$CO_2\ \text{conversion}\ (\%) = \frac{CO_{2\,\text{inlet}} - CO_{2\,\text{outlet}}}{CO_{2\,\text{inlet}}} \times 100\%$$

CH_4 selectivity and CO selectivity were calculated as following

$$CH_4\ \text{selectivity}\ (\%) = \frac{CH_{4\,\text{outlet}}}{CO_{2\,\text{inlet}} - CO_{2\,\text{outlet}}} \times 100\%$$

$$\text{CO selectivity}\ (\%) = \frac{CO_{\text{outlet}}}{CO_{2\,\text{inlet}} - CO_{2\,\text{outlet}}} \times 100\%$$

where $CO_{2\,\text{inlet}}$ and $CO_{2\,\text{outlet}}$ represent the CO_2 concentration in the feed and effluent, respectively, and $CH_{4\,\text{outlet}}$ and CO_{outlet} represent the concentration of CH_4 and CO in the effluent, respectively.

3 Results and Discussion

3.1 X-ray Diffraction (XRD)

The crystal structure of catalysts was investigated by XRD. Figure 1 shows the XRD patterns of $NiAl_2O_4$, $ZnAl_2O_4$, $NiO/ZnAl_2O_4$, $ZnO/NiAl_2O_4$ and Al_2O_3. The peaks located at 2θ of 18.9°, 31.38°, 36.67°, 44.39° and 64.88° are assigned to the (111), (220), (311), (400) and (440) planes of the cubic spinel structure of $NiAl_2O_4$ respectively (JCPDS Card no. 73-0239) [35]. The peaks located at 2θ of 18.99°, 31.69°, 37.17°, 45.26°, 49.06°, 55.66°, 59.65°, 65.62°, 74.15° and 77.33° are assigned to the (111), (220), (311), (400), (331), (422), (511), (440), (620) and (536) planes of the cubic spinel structure of $ZnAl_2O_4$ respectively (JCPDS Card no. 05-0669) [29]. For $NiO/ZnAl_2O_4$ and $ZnO/NiAl_2O_4$ samples no peaks characteristics of ZnO and NiO are seen indicating fine dispersion of these species on the $NiAl_2O_4$ and $ZnAl_2O_4$ supports respectively or may be overlapped with the supports diffraction peaks. The peaks located at 2θ of 19.86°, 32.38°, 37.85°, 46.20°, 57.40°, 61.02° and 67.12°

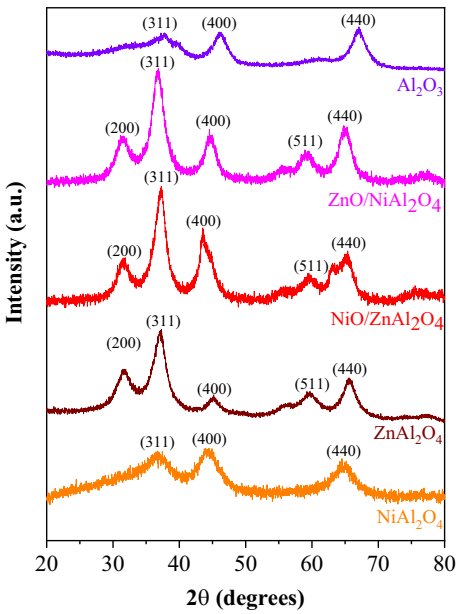

Fig. 1 XRD patterns of $NiAl_2O_4$, $ZnAl_2O_4$, $NiO/ZnAl_2O_4$, $ZnO/NiAl_2O_4$ and Al_2O_3 catalysts

Table 1 Textural parameters of the catalysts

Samples	BET surface area (m^2/g)	Pore volume (cm^3/g)	Average pore size (nm)
$NiAl_2O_4$	226	0.33	2.29
$ZnAl_2O_4$	175	0.31	1.80
$NiO/ZnAl_2O_4$	120	0.19	1.80
$ZnO/NiAl_2O_4$	94	0.13	1.80
Al_2O_3	321	0.42	2.51

are assigned to (111), (220), (311), (400), (422), (511) and (440) planes of the cubic structure of γ-Al_2O_3 [36].

3.2 N_2 Adsorption–Desorption Isotherm

The specific surface area together with the pore volume and pore size was summarized in Table 1. The N_2 adsorption–desorption isotherms of $ZnO/NiAl_2O_4$ exhibit type IV isotherm with a narrow hysteresis loop of type H3 associated with plate-like particles giving rise to slit-shaped pores [37]. However, Al_2O_3, $NiAl_2O_4$, $ZnAl_2O_4$ and $NiO/ZnAl_2O_4$ displays type IV isotherms with H2 hysteresis loop at $P/P_0 = 0.4–1.0$ associated with pores with narrow necks and wide bodies, referred to as 'ink-bottle' pores [37, 38]. The average pore size distribution is in the range of 2–25 nm indicating the presence of mesopores. After loading ZnO and NiO respectively on $NiAl_2O_4$ and $ZnAl_2O_4$, the resulting catalyst showed decreased surface area and pore volume.

3.3 TEM Analysis

The morphology and particle size of the catalysts were examined by TEM measurements and shown in Fig. 2. $NiAl_2O_4$ shows spherical shaped morphology with the size of 10 to 20 nm. $ZnAl_2O_4$ displays rod like particles. TEM images of the $NiO/ZnAl_2O_4$ and $ZnO/NiAl_2O_4$ catalysts show two separate phases of metal oxides and supports that are well mixed and dispersed which is similar to what have been reported in the literature for $NiO/NiAl_2O_4$ catalyst [39].

3.4 SEM–EDX Analysis

Table 2 summarizes the atomic percentages of various elements obtained from the SEM–EDX analyses. SEM–EDX spectra of Al_2O_3 revealed the presence of Al and O elements with the percentages of 24.21% and 75.79% respectively. All other catalysts also clearly indicates the presence of their corresponding elements.

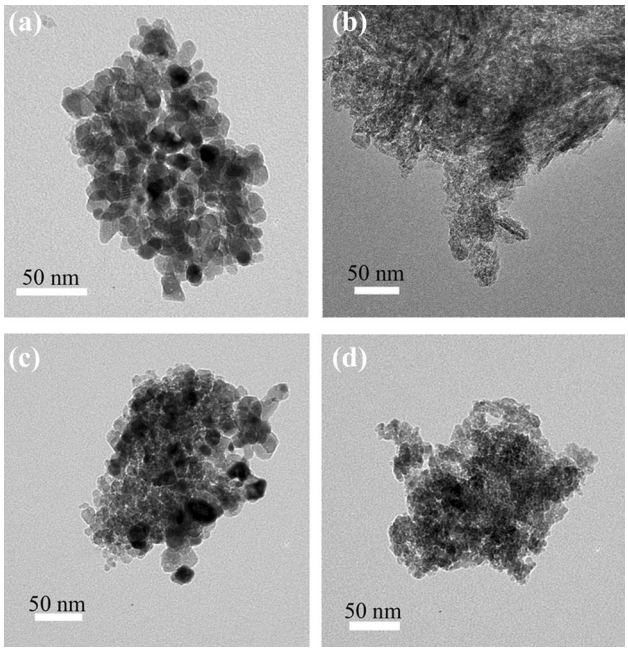

Fig. 2 TEM images of **a** $NiAl_2O_4$, **b** $ZnAl_2O_4$, **c** $NiO/ZnAl_2O_4$ and **d** $ZnO/NiAl_2O_4$

Table 2 SEM–EDX analysis of the catalysts

Catalyst	Elements, at %			
	Al	O	Ni	Zn
$NiAl_2O_4$	19.51	73.32	7.17	–
$ZnAl_2O_4$	21.50	72.19	–	6.31
$NiO/ZnAl_2O_4$	25.87	52.81	12.73	8.59
$ZnO/NiAl_2O_4$	15.48	73.60	5.11	5.81
Al_2O_3	24.21	75.79	–	–

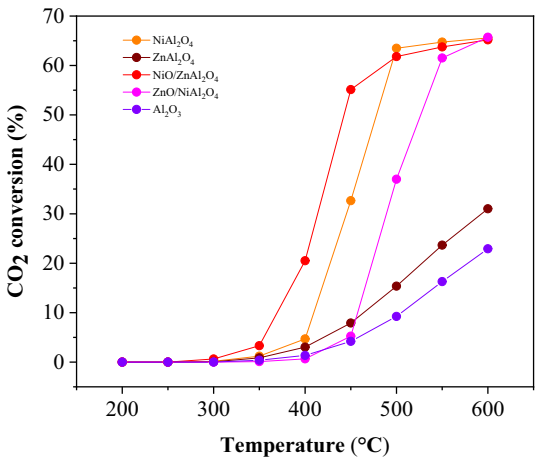

Fig. 3 CO_2 conversion as a function of temperature over $NiAl_2O_4$, $ZnAl_2O_4$, $NiO/ZnAl_2O_4$, $ZnO/NiAl_2O_4$ and Al_2O_3 catalysts

Table 3 Conversion and selectivity for CO_2 hydrogenation over various catalysts[a]

Catalysts	CO_2 conversion (%)	Selectivity (%)	
		CO	CH_4
$NiAl_2O_4$	65.57	49.60	50.40
$ZnAl_2O_4$	31.02	100	0
$NiO/ZnAl_2O_4$	65.18	53.35	46.65
$ZnO/NiAl_2O_4$	65.71	59.83	40.17
Al_2O_3	22.91	100	0

[a]Reaction conditions: T = 600 °C, $CO_2/H_2 = 1/4$, catalyst weight = 0.15 g

3.5 Catalytic Performances

To explore the catalytic performance, CO_2 hydrogenation was performed over the prepared catalysts. Figure 3 depicts the CO_2 conversion as a function of temperature over all the catalysts. CO_2 conversion and product selectivity are given in Table 3 over all the catalysts. In general, the activity of Ni containing catalysts are remarkably better than that of Zn containing catalysts and Al_2O_3 catalyst. $NiAl_2O_4$, $NiO/ZnAl_2O_4$ and $ZnO/NiAl_2O_4$ catalysts exhibit highest activity with CO_2 conversion of 65% at 600 °C, which is 2.8-fold superior in catalytic activity than that of Al_2O_3

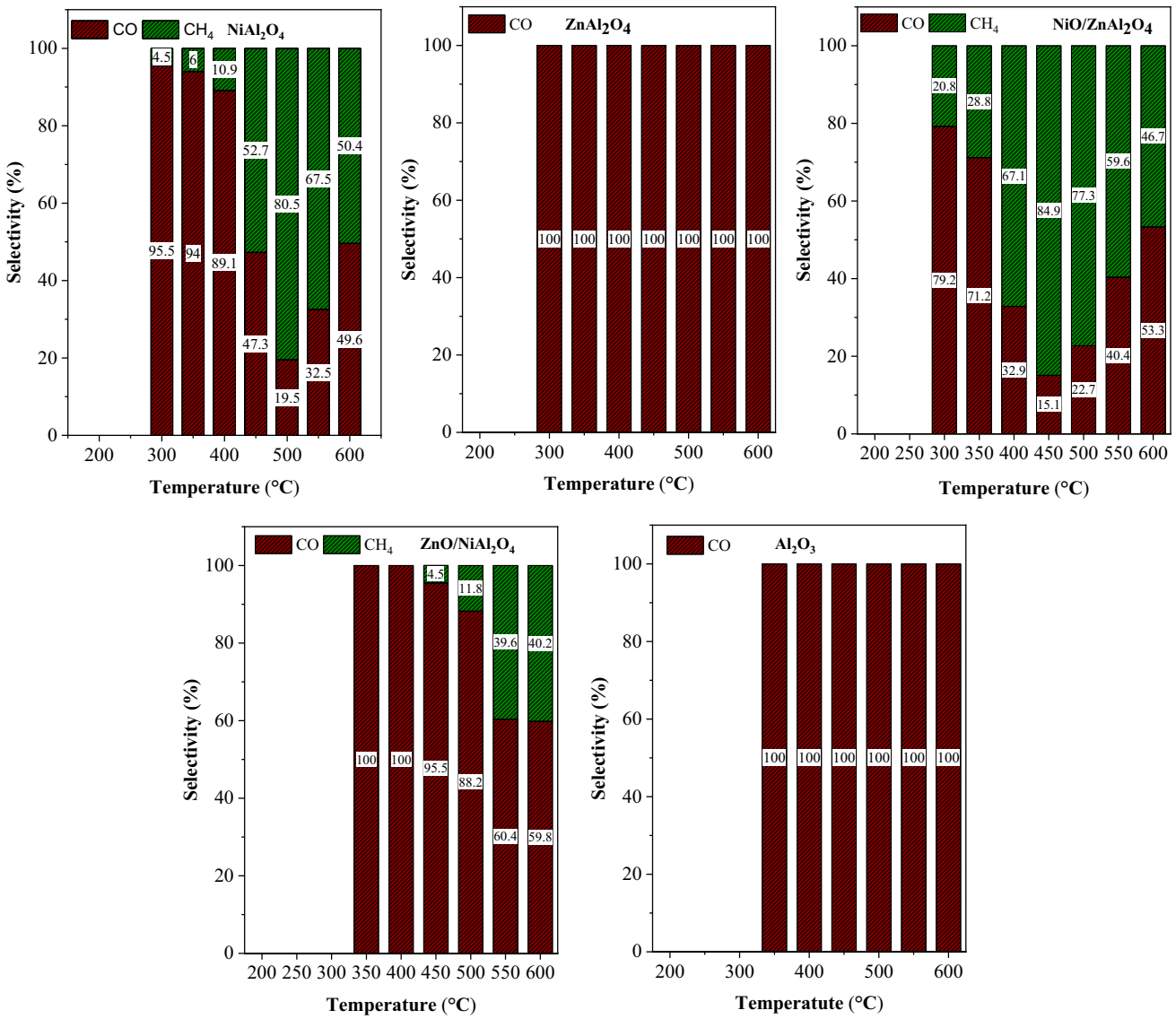

Fig. 4 Selectivity for the CO_2 hydrogenation over $NiAl_2O_4$, $ZnAl_2O_4$, $NiO/ZnAl_2O_4$, $ZnO/NiAl_2O_4$ and Al_2O_3 catalysts

Table 4 The CO_2 consumption rate (μmol/g.s) at 600 °C in CO_2 hydrogenation reaction over $NiAl_2O_4$, $ZnAl_2O_4$, $NiO/ZnAl_2O_4$, $ZnO/NiAl_2O_4$ and Al_2O_3 catalysts

Catalysts	CO_2 consumption rate (μmol/g s)
$NiAl_2O_4$	17.30
$ZnAl_2O_4$	11.24
$NiO/ZnAl_2O_4$	19.74
$ZnO/NiAl_2O_4$	18.62
Al_2O_3	7.97

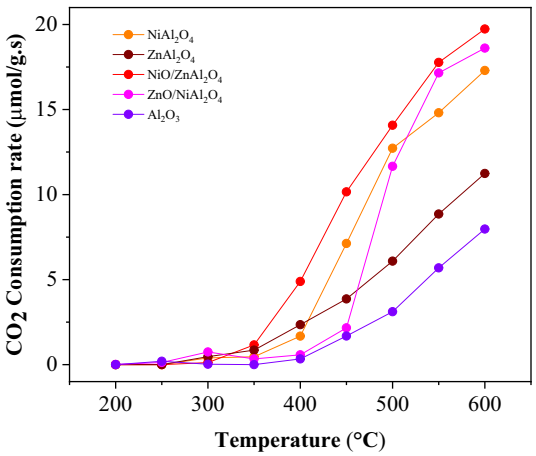

Fig. 5 CO_2 consumption rate as a function of temperature over $NiAl_2O_4$, $ZnAl_2O_4$, $NiO/ZnAl_2O_4$, $ZnO/NiAl_2O_4$ and Al_2O_3 catalysts

(Conversion = 23%) and twofold superior in catalytic activity than that of $ZnAl_2O_4$ (Conversion = 31%).

Figure 4 depicts the selectivity as a function of temperature for all the studied catalysts. The CO selectivity increases with increasing temperature due to the endothermic RWGS reaction. Among the five systems ($NiAl_2O_4$, $ZnAl_2O_4$, $NiO/ZnAl_2O_4$, $ZnO/NiAl_2O_4$ and Al_2O_3) considered in this study, the Ni containing catalysts such as $NiAl_2O_4$, $NiO/ZnAl_2O_4$ and $ZnO/NiAl_2O_4$ produced CH_4 and CO as the product but the Zn containing catalysts such as $ZnAl_2O_4$ as well as Al_2O_3 produced CO as the only product. All the nickel-containing spinels and oxide/spinel structures showed a high selectivity towards methane even at high temperature. $NiO/ZnAl_2O_4$ system has a methane selectivity of ~ 85% as well as ~ 50% at 450 °C and 600 °C, respectively.

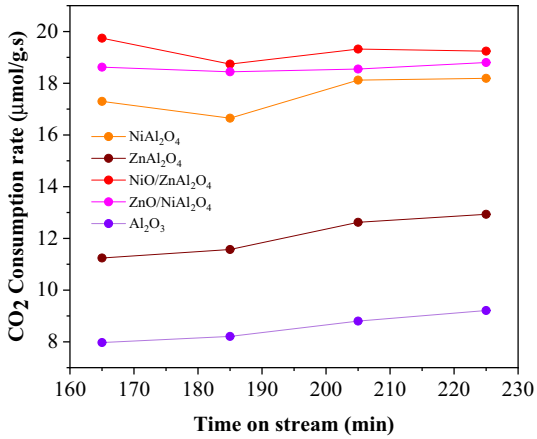

Fig. 6 Catalytic stability test over $NiAl_2O_4$, $ZnAl_2O_4$, $NiO/ZnAl_2O_4$, $ZnO/NiAl_2O_4$ and Al_2O_3 catalysts at 600 °C

The CO_2 conversion exhibit a decrease in the order: $NiO/ZnAl_2O_4 < NiAl_2O_4 < ZnO/NiAl_2O_4 < ZnAl_2O_4 < Al_2O_3$. This can be correlated with increasing Ni content. Given that an increase in Ni content can enhance CO_2 hydrogenation activity [40]. The $NiO/ZnAl_2O_4$ exhibited 65% CO_2 conversion at 600 °C with CH_4 and CO as the products. All of the Ni containing catalysts produce CH_4 as main products and CO as minor products while ZnO and other Zn containing catalysts as well as Al_2O_3 produce only CO.

Table 5 Comparative table of CO_2 consumption rate with the reported spinel catalyst for CO_2 hydrogenation

Catalysts	CO_2 conversion (%)	Catalyst weight (g)	Temperature (°C)	Flow rate of CO_2 (ml/s)	CO_2 consumption rate (μmol/g.s)	References
$NiO/ZnAl_2O_4$	65	0.15	450	0.17	10.16	This work
0.08wt%Na/$ZnFe_2O_4$	34	1	340	0.13	1.807	[46]
Co_3O_4 spinel	48	1	450	0.17	3.335	[47]
Fe(2 +) $[Fe(3+)_{0.5}Al_{0.5}]_2O_4$ spinel	40	1	320	0.12	1.962	[48]
$Cu_xZn_{1x}Al_2O_4$ spinel	4	1	250	0.42	0.687	[49]
$ZnFeO_x$-nNa	39	0.5	320	0.28	8.927	[22]
Cu–Zn–Al/SAPO-34	33	0.5	400	0.19	5.126	[50]
$ZnGa_2O_4$/SAPO-34	37	0.5	450	0.19	5.747	[50]

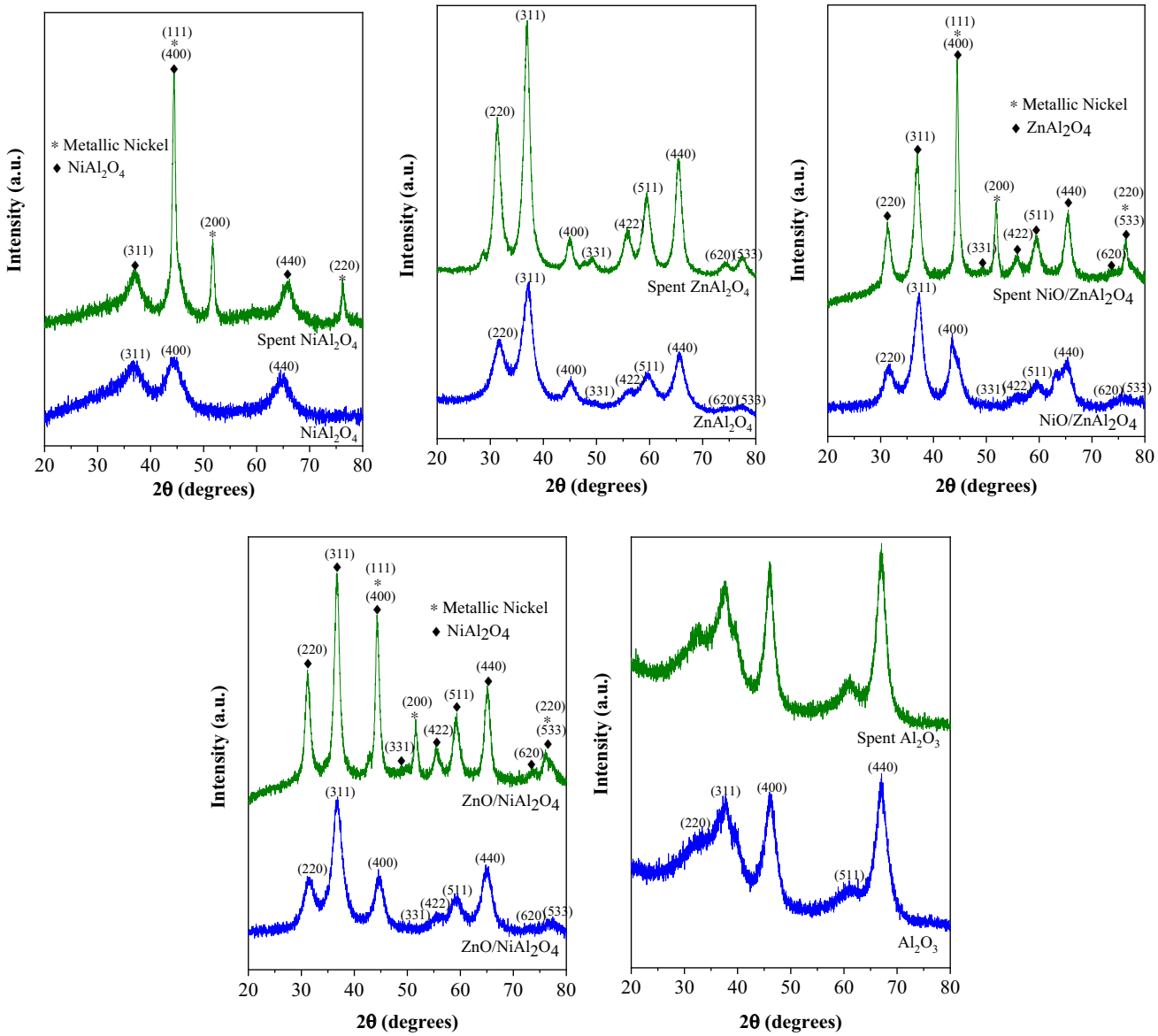

Fig. 7 XRD profiles of spent catalysts after catalytic test

In general, Ni based catalysts produce CH_4 through decomposition of formate species to CO and subsequent hydrogenation of adsorbed CO leads to the production of CH_4 [41] and ZnO is more active for the RWGS reaction [42]. Table 4 lists the CO_2 consumption rates of all the catalysts studied at 600 °C. Figure 5 depicts the CO_2 consumption rate as a function of temperature for all the studied catalysts. The CO_2 consumption rate is highest on $NiO/ZnAl_2O_4$, namely ca. 19.7 μmol h^{-1} g^{-1} at 600 °C which was 2.5 times higher than that of Al_2O_3 (ca. 7.9 μmol h^{-1} g^{-1} at 600 °C) catalyst. This catalyst also outperforms other reported spinel catalysts (Table 5) in the CO_2 hydrogenation reaction.

Although the surface area of Al_2O_3 was far higher than the $NiO/ZnAl_2O_4$, the CO_2 consumption rate was far higher on $NiO/ZnAl_2O_4$. This was due to presence of metallic Ni under reaction condition in $NiO/ZnAl_2O_4$ than in the other catalysts. Comparative table of CO_2 consumption rate of the catalyst in this study with the spinel catalyst reported in the literature for CO_2 hydrogenation is given in Table 5.

The effect of metal-support interaction was investigated over Ni/SiO_2 catalyst in the CO_2 hydrogenation reaction

[43]. It was reported that the oxygen vacancy present in the support produces surface carbon species and Ni dissociates H_2 into atomic hydrogen [44]. In the present study, the high catalytic activity of $NiO/ZnAl_2O_4$ catalyst can be attributed to the strong interaction between the Ni and the $ZnAl_2O_4$ leading to the incorporation of Ni into the $ZnAl_2O_4$ lattice and subsequent formation of oxygen vacancies [45]. This oxygen vacancies produce surface carbon species and the Ni dissociates H_2 into atomic hydrogen and forms CO and CH_4 as the final products.

3.6 Stability of the Catalyst

Figure 6 shows the stability test of all catalysts for CO_2 hydrogenation. For all the catalysts, CO_2 consumption rate had no obvious decline with time. This suggested that all the catalysts are more stable during CO_2 hydrogenation reaction. The $ZnO/NiAl_2O_4$ catalyst showed excellent catalytic stability for CO_2 hydrogenation among all the catalysts studied.

3.7 Spent Catalysts Characterization

The spent catalysts were characterized by XRD, TGA and TEM.

3.7.1 X-ray Diffraction

The spent catalysts were studied by XRD to elucidate the structural changes. The XRD of spent catalysts after catalytic test are displayed in Fig. 7. All Ni containing spent catalysts show peaks in addition to fresh ones at $2\theta = 45.39°$, 52.62° and 77° corresponding to the (111), (200) and (220) planes attributed to the metallic nickel (JCPDS No. 04-0850) [51]. However Zn containing spinels and Al_2O_3 spent catalysts showed almost no changes in their crystalline phases indicating that their crystal structures are more stable during the reaction.

3.7.2 TGA Analysis

TGA was employed to characterize the carbonaceous deposits on the spent catalysts. The TGA and DTG curves of all the spent catalysts were shown in Figs. 8 and 9 respectively. For all the spent catalysts, the weight loss below 200 °C is ascribed to desorption of adsorbed water. This weight loss is also depicted by peak starting at 50 °C and ending at 200 °C in the DTG curve as shown in Fig. 9. For Ni containing catalysts such as $NiAl_2O_4$, $NiO/ZnAl_2O_4$ and $ZnO/NiAl_2O_4$ both weight loss and weight gain were observed. The weight loss between 200 and 300 °C on $NiAl_2O_4$, $NiO/ZnAl_2O_4$ and $ZnO/NiAl_2O_4$ catalysts were 6.37%, 2.17% and 1.6% respectively. The weight gain above 300 °C on $NiAl_2O_4$, $NiO/ZnAl_2O_4$ and $ZnO/NiAl_2O_4$ catalysts were 2.44%, 4.14% and 2.91% respectively. The weight loss can be attributed to the combustion of amorphous carbon deposit and weight gain can be attributed to oxidation of metallic nickel [52, 53]. XRD also confirms the existence of considerable amount of metallic nickel in the spent catalyst (Fig. 7). As can be seen clearly in the DTG curve, the peak due to weight gain in $NiAl_2O_4$ is shifted to higher temperature in comparison to other Ni containing catalysts such as $NiO/ZnAl_2O_4$ and $ZnO/NiAl_2O_4$ indicates stronger adsorption of carbon deposits on $NiAl_2O_4$ than on $NiO/ZnAl_2O_4$ and $ZnO/NiAl_2O_4$. The weight loss on $ZnAl_2O_4$ and Al_2O_3 catalysts were 4.79% and 10.74% respectively. The weight loss between 200 and 800 °C can be attributed to the burning of carbon deposited over the catalysts [54]. Less carbon was deposited on $NiAl_2O_4$, $NiO/ZnAl_2O_4$ and $ZnO/NiAl_2O_4$ than on $ZnAl_2O_4$ and Al_2O_3 indicating Ni containing catalysts could

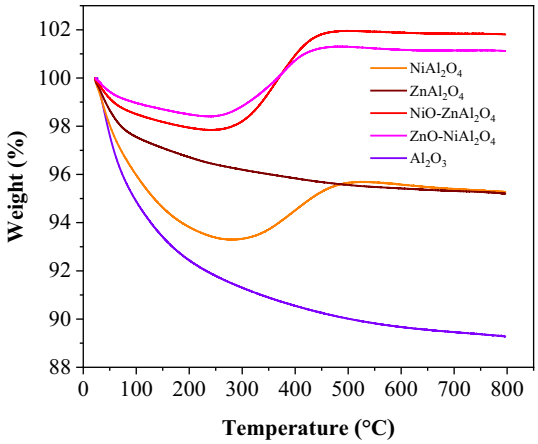

Fig. 8 TGA profiles of spent $NiAl_2O_4$, $ZnAl_2O_4$, $NiO/ZnAl_2O_4$, $ZnO/NiAl_2O_4$ and Al_2O_3 catalysts

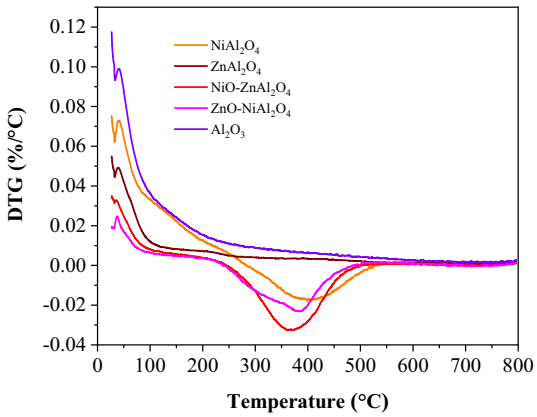

Fig. 9 DTG profiles of spent $NiAl_2O_4$, $ZnAl_2O_4$, $NiO/ZnAl_2O_4$, $ZnO/NiAl_2O_4$ and Al_2O_3 catalysts

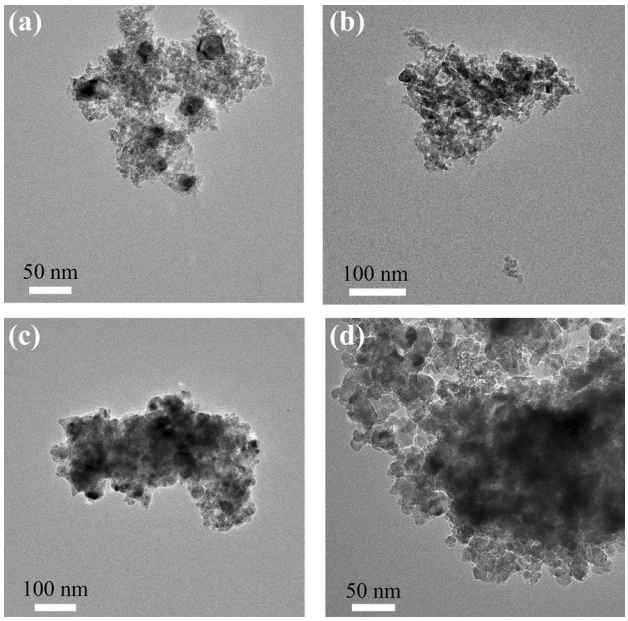

Fig. 10 TEM images of spent **a** $NiAl_2O_4$, **b** $ZnAl_2O_4$, **c** $NiO/ZnAl_2O_4$ and **d** $ZnO/NiAl_2O_4$ catalysts

effectively reduce carbon deposit. This is in line with their higher catalytic activity in CO_2 hydrogenation reaction (Table 4).

3.7.3 TEM Analysis

Figure 10 displays the TEM images of the spent $NiAl_2O_4$, $ZnAl_2O_4$, $NiO/ZnAl_2O_4$ and $ZnO/NiAl_2O_4$ catalysts. TEM images of spent catalysts reveal notable differences compared to the fresh catalysts. All the used catalysts exhibit more agglomerated particles compared to fresh catalysts. This indicates that all the catalysts were resistive towards carbon formation during the catalytic reaction.

4 Conclusion

CO_2 hydrogenation over $NiAl_2O_4$, $ZnAl_2O_4$, $NiO/ZnAl_2O_4$, $ZnO/NiAl_2O_4$ and Al_2O_3 catalysts have been investigated and it was found that $NiAl_2O_4$, $NiO/ZnAl_2O_4$ and $ZnO/NiAl_2O_4$ catalysts exhibit high activity with CO_2 conversion of 65% at 600 °C, which is several times more active compared to other catalysts reported in the literature. On the other hand, these catalysts showed a high methane selectivity even at high temperatures. The higher catalytic activity and CH_4 selectivity of $NiAl_2O_4$, $NiO/ZnAl_2O_4$ and $ZnO/NiAl_2O_4$ catalysts can be attributed to the presence of metallic Ni under the reaction conditions which can enhance the CO_2 hydrogenation activity.

Acknowledgements Open access funding provided by University of Szeged (SZTE). This paper was supported by the Hungarian Research Development and Innovation Office through grants NKFIH OTKA PD 120877 of AS. AK, and KZ is grateful for the fund of NKFIH (OTKA) K112531 & NN110676 and K120115, respectively. The financial support of the Hungarian National Research, Development and Innovation Office through the GINOP-2.3.2-15-2016-00013 project "Intelligent materials based on functional surfaces—from syntheses to applications" and the Ministry of Human Capacities through the EFOP-3.6.1-16-2016-00014 project and the, Grant 20391-3/2018/FEKUSTRAT is acknowledged.

Compliance with Ethical Standards

Conflict of interest The authors declare that they have no conflict of interest.

References

1. Wang W, Wang S, Ma X, Gong J (2011) Chem Soc Rev 40:3703–3727
2. Roy S, Cherevotan A, Peter SC (2018) ACS Energy Lett 3:1938–1966
3. Zhang X, Zhu X, Lin L, Yao S, Zhang M, Liu X, Wang X, Li Y-W, Shi C, Ma D (2016) ACS Catal 7:912–918
4. Wang F, He S, Chen H, Wang B, Zheng L, Wei M, Evans DG, Duan X (2016) J Am Chem Soc 138:6298–6305
5. Li MMJ, Chen C, Ayvalı T, Suo H, Zheng J, Teixeira IF, Ye L, Zou H, O'Hare D, Tsang SCE (2018) ACS Catal 8:4390–4401
6. Saeidi S, Najari S, Fazlollahi F, Nikoo MK, Sefidkon F, Klemeš JJ, Baxter LL (2017) Renew Sustain Energy Rev 80:1292–1311
7. Fornero EL, Chiavassa DL, Bonivardi AL, Baltanás MA (2017) J CO2 Util 22:289–298
8. Chen X, Su X, Duan H, Liang B, Huang Y, Zhang T (2017) Catal Today 281:312–318
9. Dietz L, Piccinin S, Maestri M (2015) J Phys Chem C 119:4959–4966
10. Lu X, Liu Y, He Y, Kuhn AN, Shih P-C, Sun C-J, Wen X, Shi C, Yang H (2019) ACS Appl Mater Interfaces 11:27717–27726
11. Wang W, Duong-Viet C, Ba H, Baaziz W, Tuci G, Caporali S, Nguyen-Dinh L, Ersen O, Giambastiani G, Pham-Huu C (2018) ACS Appl Energy Mater 2(2):1111–1120
12. Arandiyan H, Kani K, Wang Y, Jiang B, Kim J, Yoshino M, Rezaei M, Rowan AE, Dai H, Yamauchi Y (2018) ACS Appl Mater Interfaces 10:24963–24968
13. Rungtaweevoranit B, Baek J, Araujo JR, Archanjo BS, Choi KM, Yaghi OM, Somorjai GA (2016) Nano Lett 16:7645–7649

14. Bahruji H, Bowker M, Hutchings G, Dimitratos N, Wells P, Gibson E, Jones W, Brookes C, Morgan D, Lalev G (2016) J Catal 343:133–146
15. Huš M, Dasireddy VD, Štefančič NS, Likozar B (2017) Appl Catal B Environ 207:267–278
16. Dasireddy VD, Likozar B (2019) Renew Energy 140:452–460
17. Huš M, Kopač D, Štefančič NS, Jurković DL, Dasireddy VD, Likozar B (2017) Catal Sci Technol 7:5900–5913
18. Huang X, Wang P, Zhang Z, Zhang S, Du X, Bi Q, Huang F (2019) New J Chem 43:13217–13224
19. Branco JB, Brito PE, Ferreira AC (2019) Chem Eng J 380:122465
20. Le TA, Kim J, Jeong YR, Park ED (2019) Catalysts 9:599
21. Bahmanpour AM, Héroguel F, Kılıç M, Baranowski C, Artiglia L, Rothlisberger U, Luterbacher JS, Kröcher O (2019) ACS Catal 9(7):6243–6251
22. Cui X, Gao P, Li S, Yang C, Liu Z, Wang H, Zhong L, Sun Y (2019) ACS Catal 9:3866–3876
23. Salleh N, Jalil A, Triwahyono S, Efendi J, Mukti R, Hameed B (2015) Appl Surf Sci 349:485–495
24. Vijaya JJ, Kennedy LJ, Sekaran G, Jeyaraj B, Nagaraja K (2008) J Hazard Mater 153:767–774
25. Rahman MA, Ahamed E, Faruque MRI, Islam MT (2018) Sci Rep 8:14948
26. García-Lario AL, Aznar M, Martinez I, Grasa GS, Murillo R (2015) Int J Hydrogen Energy 40:219–232
27. Kathiraser Y, Thitsartarn W, Sutthiumporn K, Kawi S (2013) J Phys Chem C 117:8120–8130
28. Le Peltier F, Chaumette P, Saussey J, Bettahar M, Lavalley J (1998) J Mol Catal A Chem 132:91–100
29. Liu J, Zhou W, Jiang D, Wu W, Miao C, Wang Y, Ma X (2018) Ind Eng Chem Res 57:11265–11270
30. Wang A, Wang J, Lu C, Xu M, Lv J, Wu X (2018) Fuel 234:430–440
31. Zhao L, Bi S, Pei J, Li X, Yu R, Zhao J, Martyniuk CJ (2016) J Ind Eng Chem 41:151–157
32. Mulwa W, Dejene B, Onani M, Ouma C (2017) J Lumin 184:7–16
33. Okal J, Zawadzki M (2013) Appl Catal A Gen 453:349–357
34. Zhou W, Kang J, Cheng K, He S, Shi J, Zhou C, Zhang Q, Chen J, Peng L, Chen M (2018) Angew Chem 130:12188–12192
35. Sun Y, Jiang E, Xu X, Wang J, Li Z (2018) ACS Sustain Chem Eng 6:14660–14668
36. Sun J, Wang Y, Zou H, Wang Z-J, Guo X (2019) J Energy Chem 29:3–7
37. Sing KS (1985) Pure Appl Chem 57:603–619
38. Shamskar FR, Rezaei M, Meshkani F (2017) Int J Hydrogen Energy 42:4155–4164
39. Wang C, Chen Y, Cheng Z, Luo X, Jia L, Song M, Jiang B, Dou B (2015) Energy Fuels 29:7408–7418
40. Heine C, Lechner BA, Bluhm H, Salmeron M (2016) J Am Chem Soc 138:13246–13252
41. Jia X, Zhang X, Rui N, Hu X (2019) Liu C-j. Appl Catal B Environ 244:159–169
42. Park S-W, Joo O-S, Jung K-D, Kim H, Han S-H (2001) Appl Catal A Gen 211:81–90
43. Wu H, Chang Y, Wu J, Lin J, Lin I, Chen C (2015) Catal Sci Technol 5:4154–4163
44. Aziz M, Jalil A, Triwahyono S, Mukti R, Taufiq-Yap Y, Sazegar M (2014) Appl Catal B Environ 147:359–368
45. Andraos S, Abbas-Ghaleb R, Chlala D, Vita A, Italiano C, Laganà M, Pino L, Nakhl M, Specchia S (2019) Int J Hydrogen Energy 44:25706–25716
46. Choi YH, Ra EC, Kim EH, Kim KY, Jang YJ, Kang KN, Choi SH, Jang JH, Lee JS (2017) Chemsuschem 10:4764–4770
47. Kierzkowska-Pawlak H, Tracz P, Redzynia W, Tyczkowski J (2017) J CO2 Util 17:312–319
48. Utsis N, Vidruk-Nehemya R, Landau M, Herskowitz M (2016) Faraday Discuss 188:545–563
49. Conrad F, Massue C, Kühl S, Kunkes E, Girgsdies F, Kasatkin I, Zhang B, Friedrich M, Luo Y, Armbrüster M (2012) Nanoscale 4:2018–2028
50. Liu X, Wang M, Zhou C, Zhou W, Cheng K, Kang J, Zhang Q, Deng W, Wang Y (2018) Chem Commun 54:140–143
51. Song S, Yao S, Cao J, Di L, Wu G, Guan N, Li L (2017) Appl Catal B Environ 217:115–124
52. Li S, Tang H, Gong D, Ma Z, Liu Y (2017) Catal Today 297:298–307
53. Bian L, Wang W, Xia R, Li Z (2016) RSC Adv 6:677–686
54. Charisiou ND, Douvartzides SL, Siakavelas GI, Tzounis L, Sebastian V, Stolojan V, Hinder SJ, Baker MA, Polychronopoulou K, Goula MA (2019) Catalysts 9:676